Mon. Not. R. Astron. Soc. **351,** 826–844 (2004) doi:10.1111/j.1365-2966.2004.07827.x

Photospheric magnetic field and surface differential rotation of the FK Com star HD 199178

P. Petit,[1,2⋆] J.-F. Donati,[2⋆] J. M. Oliveira,[3⋆] M. Aurière,[2⋆] S. Bagnulo,[4⋆] J. D. Landstreet,[5⋆] F. Lignières,[2⋆] T. Lüftinger,[6⋆] S. Marsden,[2⋆] D. Mouillet,[2⋆] F. Paletou,[2⋆] S. Strasser,[7⋆] N. Toqué[2⋆] and G. A. Wade[8⋆]

[1]*Centro de Astrofisica da Universidade do Porto, rua das Estrelas, 4150-762 Porto, Portugal*
[2]*Laboratoire d'Astrophysique, Observatoire Midi-Pyrénées, 14 Av. E. Belin, F–31400 Toulouse, France*
[3]*School of Chemistry and Physics, Keele University, Staffordshire ST5 5BG*
[4]*European Southern Observatory, Alonso de Cordova 3107, Vitacura, Santiago, Chile*
[5]*Department of Physics and Astronomy, The University of Western Ontario, London, Ontario, Canada N6G 3K7*
[6]*Institut für Astronomie, Tuerkenschanzstrasse 17, A-1180 Wien, Austria*
[7]*Department of Physics and Astronomy, University of Calgary, Calgary, Alberta, Canada T2N 1N4*
[8]*Royal Military College of Canada, Department of Physics, PO Box 17000, Station 'Forces', Kingston, Ontario, Canada K7K 4B4*

Accepted 2004 March 8. Received 2004 March 4; in original form 2004 January 16

ABSTRACT

We present spectropolarimetric observations of the FK Com star HD 199178 obtained between 1998 December and 2003 August at the Télescope Bernard Lyot (Observatoire du Pic du Midi, France). We report the detection of a photospheric magnetic field and reconstruct its distribution by means of Zeeman–Doppler imaging. We observe large regions where the magnetic field is mainly azimuthal, suggesting that the dynamo processes generating the magnetic activity of HD 199178 may be active very close to the stellar surface. We investigate the rapid evolution of surface brightness and magnetic structures from a continuous monitoring of the star over several weeks in 2002 and 2003. We report that significant changes occur in the distribution of cool-spots and magnetic regions on typical time-scales of the order of two weeks. Our spectropolarimetric observations also suggest that the surface of HD 199178 is sheared by differential rotation, with a difference in rotation rate between equatorial and polar regions of the order of 1.5 times that of the Sun.

Key words: magnetic fields – polarization – stars: activity – stars: imaging – stars: individual: HD 199178 – stars: rotation.

1 INTRODUCTION

Our understanding of the solar dynamo has benefited from important progress during the last decade, thanks to the combined breakthroughs of observational and modelling techniques. Helioseismological studies are now able to reveal the internal velocity field of the Sun (Schou et al. 1998) and recent magnetohydrodynamic (MHD) simulations give credence to the idea that the dynamo processes at the origin of the large-scale solar field are mainly operating within a thin interface layer separating the radiative core from the convective envelope of the Sun: the tachocline. This region allows an efficient transformation of a seed poloidal field into a toroidal component as well as storage of the field on a time-scale of the order of the solar magnetic cycle (Rempel, Schüssler & Tóth 2000). The poloidal component of the field is believed to be regenerated (with opposite polarity) through the action of the Coriolis force, by means of a still mostly unknown mechanism called the 'α-effect', which may also be mostly efficient within the tachocline (Dikpati & Gilman 2001).

The magnetic field observed at the photospheric level of the Sun was first detected in sunspots (Hale 1908) which are the largest magnetic structures of the solar surface (though only covering about 10^{-4} of the photosphere at solar maximum), featuring mostly radially oriented field lines. Magnetic elements are now observed at much smaller scales in the so-called quiet photosphere (see Solanki 2001, for a review of the properties of such magnetic regions). The interplay, during the solar cycle, between the small magnetic structures and the large-scale field has not yet been understood, whereas small

⋆petit@astro.up.pt (PP); donati@ast.obs-mip.fr(J-FD); auriere@ast.obs-mip.fr (MA); francois.lignieres@obs-mip.fr (FL); marsden@ast.obs-mip.fr (SM); mouillet@bagn.obs-mip.fr (DM); toque@ast.obs-mip.fr(NT); joana@astro.keele.ac.uk (JMO); sbagnulo@eso.org (SB); jlandstr@astro.uwo.ca (JDL); theresa@tycho.astro.univie.ac.at (TL); strasser@ras.ucalgary.ca (SS); Gregg.Wade@rmc.ca (GAW)

magnetic elements store a significant part of the magnetic energy of the photosphere, and despite the fact that the distribution of some of these structures has a temporal evolution correlated to the solar cycle. Some studies also suggest that a turbulent dynamo, disconnected from the large-scale solar dynamo, may efficiently generate small-scale magnetic structures (Cattaneo 1999).

Surprisingly, these properties of the solar photospheric field are far from the general features observed on other active stars, at least among the fast-rotator group. The surface magnetic field of several fast-rotating stars has been mapped by means of Zeeman–Doppler Imaging (hereafter ZDI, Semel 1989). For these extremely active objects, a field is generally observed at basically all locations of the photosphere (see e.g. Donati et al. 2003a), in the form of discrete structures that present a homogeneous orientation of field lines and cover a significant fraction of the stellar surface. On some objects, the surface field is dominated by an azimuthal component distributed in arcs or even in complete rings encircling the rotation axis at different latitudes. These observations suggest that the dynamo operating within these objects is very different from that of the Sun, since the azimuthal component of the solar field is supposed to be deeply buried at the base of the convective envelope. Its presence at the photospheric level on fast rotators therefore suggests that their dynamo may be active very close to the surface.

The observing effort engaged during the last decade to investigate, by means of high-resolution spectropolarimetry, the magnetic activity of active late-type fast rotators has been concentrated on several pre-main-sequence stars and on the evolved close binary system HR 1099. The present study focuses on HD 199178, a member of the small FK Com group. Objects belonging to this class are single fast-rotating late-type giants displaying signs of strong magnetic activity. Their short rotation periods (of order of a few days) suggest that FK Com stars have undergone very unusual mechanisms during their evolution. In particular, it was proposed by Bopp & Stencel (1981) that they may result from the coalescence of contact binaries. Long-term photometric studies of FK Com itself (Jetsu et al. 1991; Korhonen, Berdyugina & Tuominen 2002) report that its cool-spot distribution is asymmetric (a so-called 'active longitude' dominating the spot activity), with occasional 180° shifts of the active longitude (behaviour dubbed 'flip-flop') resulting in a 6.5-yr cycle. The distribution of cool-spots of HD 199178 has also been investigated by means of Doppler imaging (Strassmeier et al. 1999; Hackman, Jetsu & Tuominen 2001).

The aim of the present study is to enrich our knowledge of this object by reconstructing its magnetic topology together with its spot distribution, in a twofold purpose. We first plan to compare the general properties of the photospheric magnetic field of this evolved star with the magnetic topologies mapped for younger objects. We also intend to check whether active longitudes reported by Hackman et al. (2001) are also observed in our own maps of the cool-spot distribution and test whether they have a counterpart in the magnetic images.

We first summarize the series of spectropolarimetric observations used for this study and describe the modelling procedures employed to reconstruct the magnetic topology of the star at every observing epoch. We then present the main characteristics of its surface brightness and magnetic structures and study their evolution on different time-scales (from a few weeks to several years), including an analysis of the surface differential rotation. We finally summarize the main results and outline the information they provide on the nature of the underlying dynamo processes.

2 OBSERVATIONS, DATA REDUCTION AND IMAGING PROCEDURE

2.1 Observations

All the spectropolarimetric data presented in this article were obtained with the MuSiCoS spectrograph (Baudrand & Böhm 1992) fibre fed by its Cassegrain-mounted polarimetric module (Donati et al. 1999). The data reduction, performed with ESpRIT (Donati et al. 1997), is similar to that described by Petit et al. (2004) for HR 1099, including the additional wavelength calibration using telluric lines. The data sets (listed in Tables 1 and 2) were obtained between 1998 December and 2003 August, yielding a total number of 380 brightness spectra and 94 circularly polarized spectra.

Least-square deconvolution (hereafter LSD, Donati et al. 1997) was employed to perform a simultaneous extraction of the signal from all photospheric spectral features of the echelograms. A line mask corresponding to a G5 spectral type (Strassmeier et al. 1999) yielded a multiplex gain of the order of 30 for the Stokes V profiles. The signal-to-noise ratio (S/N) of LSD Stokes I profiles is limited to about 1100 at best, indicating that the convolution model underlying LSD cannot be trusted above this accuracy level. Depending on data quality, the multiplex gain undergoes small fluctuations, so that raw spectra of equal S/N can produce LSD profiles with slightly different noise levels.

The data quality of different observing periods is very uneven (due to weather conditions), so that the S/N of LSD profiles ranges from about 3600 (in average in 2001 July) to more than 7000 on 2003 July 31 (in optimal seeing and transparency conditions). The large data sets of the summers of 2002 and 2003 are split into several subsets (separated by blank lines in Tables 1 and 2). Each subset is used to reconstruct an individual brightness and magnetic image of the star (Section 2.2), ensuring that each map is computed from observations obtained over a time-span consistent with the typical short-term evolution of photospheric structures (Section 3.3).

2.2 Imaging procedure

All magnetic images described hereafter are obtained with the ZDI code developed by Brown et al. (1991) and Donati & Brown (1997), following the maximum entropy image reconstruction algorithm of Skilling & Bryan (1984). This imaging procedure was tested for various stellar parameters and observing conditions by Donati & Brown (1997), from a series of numerical simulations. They demonstrated that the orientation of field lines within magnetic regions can be accurately reconstructed for noise levels similar to that available in the present study and for inclination angles of the rotation axis similar to that derived later in this section for HD 199178. However, in the case of images reconstructed with data presenting an incomplete phase sampling of the star, only a partial reconstruction of the magnetic field is achieved, containing radial/meridional field regions closest to the observed longitudes and azimuthal field structures located about 0.1 rotation cycle away from the observed longitudes. With sparse phase coverage, the reconstructed position of active regions located next to phase gaps can also be slightly shifted toward higher latitudes and unobserved phases (Petit, Donati & Cameron 2002). Comparisons between ZDI images of HR 1099 reported by Donati et al. (2003a) and Petit et al. (2003) demonstrate, however, that maps of the same object obtained with simultaneous observations, but with different instrumental set-ups, are very consistent despite very different noise levels and phase sampling.

Table 1. Journal of observations from 1998 December to 2002 July. Each line corresponds to a full polarization cycle. Columns 2 and 3 list the date and hour of observation (first and last exposure of the cycle). Column 4 contains the number of unpolarized/polarized exposures. Column 5 lists the total exposure time of each Stokes I individual subexposure. We also list the S/N ratios (per 4 km s^{-1} velocity bins) of the unpolarized and polarized spectra (in columns 6 and 8, respectively, with minimum and maximum values in the sequence) and in the associated mean LSD profiles (columns 7 and 9). The multiplex gain between the raw polarized spectra and the mean Stokes V profiles is reported in the last column.

Date	JD (+2,450,000)	UT (hh:mm:ss)	nexp	t_{exp} (s)	S/N I	S/N I_{LSD}	S/N V	S/N V_{LSD}	multiplex gain V
1998 Dec 5	1153.29/1153.32	18:58:31/19:34:00	4/1	600	90/100	1053/1072	180	5509	31
1999 Jan 14	1193.25/1193.27	18:00:57/18:34:16	4/1	600	80/90	759/855	170	4690	28
1999 Jan 18	1197.25/1197.27	18:00:59/18:34:38	4/1	600	100/100	1074/1081	190	4997	26
1999 Jan 19	1198.25/1198.27	18:02:20/18:35:28	4/1	600	90/100	970/1018	170	4599	27
2001 Jul 3	2094.44/2094.49	22:38:11/23:51:16	5/1	900	60/100	966/1066	190	5873	31
2001 Jul 7	2098.45/2098.48	22:41:03/23:34:41	4/1	145/900	30/90	686/1069	150	2908	19
2001 Jul 18	2109.46/2109.49	23:06:23/23:41:08	3/1	900	20/30	435/556	34	768	23
2001 Jul 25	2115.53/2115.56	00:37:14/01:24:35	4/1	900	50/60	838/937	110	2824	26
2001 Jul 26	2117.41/2117.44	21:46:48/22:34:10	4/1	900	100/100	1062/1091	200	5820	29
2001 Dec 1	2245.26/2245.29	18:16:05/19:03:26	4/1	900	70/80	897/1038	140	3895	28
2001 Dec 2	2246.23/2246.26	17:33:05/18:20:26	4/1	900	100/100	1053/1070	190	5556	29
2001 Dec 7	2251.23/2251.26	17:31:59/18:19:20	4/1	900	100/100	1053/1066	190	5463	29
2001 Dec 8	2252.23/2252.27	17:35:20/18:22:41	4/1	900	90/100	1063/1073	180	5325	30
2001 Dec 9	2253.23/2253.27	17:36:42/18:24:04	4/1	900	100/110	1072/1078	200	6064	30
2001 Dec 10	2254.24/2254.27	17:43:08/18:30:30	4/1	900	80/100	1024/1073	170	5061	30
2001 Dec 11	2255.24/2255.27	17:42:24/18:29:45	4/1	900	100/110	1056/1071	210	6206	30
2001 Dec 12	2256.24/2256.27	17:38:59/18:26:21	4/1	900	100/110	1065/1088	210	6310	30
2001 Dec 13	2257.24/2257.27	17:38:55/18:26:16	4/1	900	170/180	754/882	220	6844	31
2001 Dec 16	2260.24/2260.27	17:39:23/18:26:44	4/1	900	90/100	1047/1157	180	5087	28
2002 Jun 11	2437.47/2437.51	23:10:02/23:59:11	4/1	900	60/80	982/1045	130	3486	27
2002 Jun 12	2438.48/2438.51	23:31:33/00:18:55	4/1	900	40/60	827/941	98	2485	25
2002 Jun 13	2439.49/2439.52	23:39:48/00:27:12	4/1	900	70/90	909/1054	160	4497	28
2002 Jun 15	2441.47/2441.51	23:16:34/00:07:37	4/1	900	80/90	1043/1075	170	5081	30
2002 Jun 18	2444.41/2444.44	21:49:48/22:37:09	4/1	900	60/90	933/1064	130	3801	29
2002 Jun 22	2448.45/2448.48	22:41:35/23:28:56	4/1	900	100/110	1090/1111	210	6126	29
2002 Jun 25	2451.40/2451.44	21:40:20/22:27:43	4/1	900	90/100	1062/1090	170	4993	29
2002 Jun 28	2454.43/2454.46	22:20:47/23:08:00	4/1	900	80/100	1037/1109	180	4842	27
2002 Jun 29	2454.57/2454.60	01:39:51/02:27:12	4/1	900	40/100	814/1090	160	3485	22
2002 Jun 29	2455.42/2455.45	22:05:59/22:53:20	4/1	900	70/90	991/1055	160	4474	28
2002 Jun 30	2455.57/2455.60	01:42:08/02:29:29	4/1	900	80/100	1006/1086	190	5378	28
2002 Jul 1	2457.50/2456.53	00:00:31/00:47:53	4/1	900	70/80	937/1036	130	3625	28
2002 Jul 2	2458.43/2458.46	22:18:02/23:05:23	4/1	900	70/70	1013/1031	130	3728	29
2002 Jul 3	2458.53/2458.56	00:42:02/01:29:23	4/1	900	60/70	968/1004	120	3199	27
2002 Jul 4	2459.55/2459.59	01:15:22/02:02:43	4/1	900	60/70	909/1002	120	3550	30
2002 Jul 4	2460.42/2460.45	22:02:50/22:50:11	4/1	900	50/60	924/995	110	2971	27
2002 Jul 5	2460.52/2460.55	00:24:40/01:12:01	4/1	900	60/70	992/1024	130	3514	27
2002 Jul 5	2460.62/2460.65	02:55:48/03:43:09	4/1	900	80/100	1057/1083	160	4769	30
2002 Jul 11	2467.41/2467.44	21:45:13/22:32:38	4/1	900	70/80	989/1045	140	3653	26
2002 Jul 12	2467.54	00:56:31	1/0	900	80	1033	–	–	–
2002 Jul 17	2473.41/2473.44	21:44:56/22:32:12	4/1	900	140/150	715/817	300	4215	14
2002 Jul 17	2473.49/ 2473.52	23:44:49/00:32:04	4/1	900	100/110	630/675	210	3293	16
2002 Jul 18	2474.44/ 2474.48	22:40:41/ 23:27:58	4/1	900	30/50	589/838	76	1833	24
2002 Jul 19	2474.58/2474.61	01:51:52/02:39:8	4/1	900	40/60	765/974	94	2384	25
2002 Jul 19	2475.40/2475.44	21:42:56/22:30:12	4/1	900	30/50	660/828	82	1934	24
2002 Jul 19	2475.45/2475.48	22:50:32/23:37:47	3/0	900	30/50	509/878	–	–	–
2002 Jul 21	2477.49/2477.52	23:44:47/00:32:26	4/1	900	70/70	945/970	120	3225	27
2002 Jul 22	2477.59/2477.62	02:04:22/02:52:02	4/1	900	70/80	998/1052	140	3742	27
2002 Jul 26	2482.43/2482.47	22:22:46/23:10:01	4/1	900	80/80	1040/1045	150	4034	27
2002 Jul 27	2482.53/2482.56	00:41:53/01:29:08	4/1	900	70/80	972/1048	150	4102	27
2002 Jul 27	2482.63/2482.67	03:14:15/04:01:30	4/1	900	100/100	1062/1091	200	5941	30
2002 Jul 27	2483.43/2483.46	22:15:20/23:02:35	4/1	900	100/100	1038/1092	190	5617	30
2002 Jul 28	2483.52/2483.56	00:34:07/01:21:23	4/1	900	90/90	1051/1075	180	5077	28
2002 Jul 28	2483.63/2483.66	03:5:23/03:52:39	4/1	900	90/100	1041/1083	180	4980	28

Table 2. Same as Table 1 for summer 2003 observations.

Date	JD (+2,450,000)	UT (hh:mm:ss)	nexp	t_{exp} (s)	S/N I	S/N I_{LSD}	S/N V	S/N V_{LSD}	multiplex gain V
2003 Jun 27	2817.58/2817.61	01:55:40/02:38:20	4/1	800	100/100	1095/1101	200	6053	30
2003 Jun 29	2819.59/2819.62	02:10:10/02:52:50	4/1	800	70/80	1031/1042	140	3953	28
2003 Jul 4	2825.48/2825.51	23:34:01/00:16:42	4/1	800	90/100	1077/1104	170	4787	28
2003 Jul 6	2826.59/2826.62	02:03:18/02:45:58	4/1	800	60/90	930/1074	140	3825	27
2003 Jul 7	2827.53/2827.56	00:37:50/01:20:30	4/1	800	100/100	1076/1083	190	5528	29
2003 Jul 8	2828.50/2828.53	24:06:10/00:48:50	4/1	800	70/80	993/1037	130	3773	29
2003 Jul 10	2830.55/2830.58	01:11:40/01:54:20	4/1	800	90/100	1010/1086	180	5382	30
2003 Jul 11	2831.54/2831.57	00:59:25/01:42:06	4/1	800	60/90	892/1030	130	3749	29
2003 Jul 12	2832.58/2832.61	01:52:08/02:34:48	4/1	800	90/110	1080/1090	190	5550	29
2003 Jul 12	2833.46/2833.49	23:06:00/23:48:42	4/1	800	80/90	1051/1058	160	4465	28
2003 Jul 15	2835.57/2835.60	01:37:13/02:19:29	4/1	800	70/90	1054/1081	160	4610	29
2003 Jul 17	2837.57/2837.60	01:39:30/02:21:51	4/1	800	50/70	905/1035	120	3383	28
2003 Jul 17	2838.47/2838.50	23:18:50/24:01:00	4/1	800	70/80	1027/1063	150	4281	29
2003 Jul 18	2839.46/2839.49	23:04:30/23:46:46	4/1	800	80/90	1016/1065	160	4716	29
2003 Jul 19	2840.45/2840.48	22:53:17/23:35:32	4/1	800	90/100	1034/1081	180	5268	29
2003 Jul 20	2841.46/2841.49	23:07:40/23:49:55	4/1	800	80/80	1039/1058	150	4310	29
2003 Jul 21	2841.59/2841.62	02:12:15/02:54:31	4/1	800	70/80	973/1032	130	3893	30
2003 Jul 22	2842.55/2842.58	01:16:28/01:58:44	4/1	800	100/100	1102/1093	90	5607	29
2003 Jul 22	2843.46/2843.48	22:55:15/23:37:31	4/1	800	90/100	1061/1074	180	5412	30
2003 Jul 23	2843.55/2843.58	01:13:27/01:55:44	4/1	800	100/100	1074/1088	190	5540	29
2003 Jul 23	2844.45/2844.48	22:46:45/23:29:01	4/1	800	100/100	1078/1096	190	5686	30
2003 Jul 24	2844.55/2844.58	01:08:41/01:50:57	4/1	800	10/90	268/1072	110	1162	11
2003 Jul 24	2845.47/2845.50	23:17:32/23:59:48	4/1	800	90/90	1068/1084	170	4988	29
2003 Jul 25	2845.59/2845.62	02:06:23/02:48:39	4/1	800	80/80	1033/1051	150	4315	29
2003 Jul 25	2846.47/2846.50	23:13:19/23:55:35	4/1	800	40/80	740/1034	110	2806	25
2003 Jul 27	2847.60/2847.63	02:21:46/03:04:00	4/1	800	60/90	979/1069	140	4196	30
2003 Jul 27	2848.45/2848.48	22:51:13/23:33:28	4/1	800	70/80	1025/1053	140	4130	29
2003 Jul 28	2848.58/2848.61	01:57:30/02:39:46	4/1	800	80/90	1049/1077	160	4784	30
2003 Jul 29	2849.54/2849.57	01:00:45/01:43:01	4/1	800	110/110	1103/1107	220	6718	30
2003 Jul 29	2850.41/2850.44	21:47:58/22:30:14	4/1	800	100/110	1014/1118	210	6399	30
2003 Jul 30	2850.58/2850.61	02:01:36/02:43:51	4/1	800	100/110	1050/1104	210	6405	30
2003 Jul 30	2851.41/2851.44	21:45:27/22:27:43	4/1	800	90/90	1022/1087	180	5305	29
2003 Jul 31	2851.53/2851.56	00:42:03/01:29:18	4/1	900	100/110	1081/1113	200	6003	30
2003 Jul 31	2852.41/2852.44	21:54:40/22:36:56	4/1	800	110/120	1041/1108	230	7090	31
2003 Aug 1	2852.59/2852.62	02:10:05/02:52:21	4/1	800	110/110	987/1120	220	6669	30
2003 Aug 3	2854.54/2854.57	00:52:43/01:34:59	4/1	800	110/110	959/1114	210	6483	31
2003 Aug 3	2854.58/2854.61	01:49:01/02:31:17	4/1	800	110/110	980/1096	220	6548	30
2003 Aug 4	2855.55/2855.58	01:09:28/01:51:44	4/1	800	90/90	971/1020	160	4419	28
2003 Aug 4	2855.59/2855.62	02:05:47/02:48:03	4/1	800	80/90	910/984	170	4831	28
2003 Aug 4	2856.46/2856.49	23:08:58/23:51:14	4/1	800	100/100	1084/1107	200	5936	30
2003 Aug 5	2856.60/2856.63	02:30:45/03:13:01	4/1	800	80/100	936/1035	180	5160	29
2003 Aug 5	2857.48/2857.51	23:34:09/00:16:25	4/1	800	100/110	1002/1088	200	6033	30
2003 Aug 6	2857.56/2857.59	01:24:59/02:07:15	4/1	800	100/110	1061/1094	210	6398	30

We model the photospheric brightness inhomogeneities by means of the two-component description of Cameron (1992). The average intrinsic profile used for computing brightness images is a synthetic Gaussian line reproducing the characteristics of a MuSiCoS LSD Stokes I profile of the K0 star β Gem. This option was adopted according to the results of Unruh & Cameron (1995), who demonstrated that Doppler images reconstructed from a Gaussian line were almost indistinguishable from that obtained using a standard star. The template profile was scaled by a factor 0.5 and 1, for the spotted areas and the quiet photosphere, respectively, to mimic the different LSD signatures expected from these two regions (Donati & Cameron 1997). The adopted temperatures are 5500 K and 4000 K, respectively, for the quiet photosphere and the spotted regions, both values being close to that determined by O'Neal, Neff & Saar (1998) from TiO band modelling.

The large volume of data we collected for the present study allows us to obtain estimates of the imaging parameters associated with HD 199178. To estimate the radial velocity v_{rad}, we reconstruct several images from the same data set, tuning the value of v_{rad} and choosing the one that minimizes the information content of the image (following Cameron & Unruh 1994). In order to estimate the projected rotational velocity $v \sin i$, we prefer to adopt the more reliable estimate provided by a classical fit to the data (Donati et al. 2003a), from which we can obtain a better adjustment of the wings of the profiles, at the cost of a slightly higher spot (or magnetic field) coverage. The values we obtain for v_{rad} and $v \sin i$ are, respectively, equal to -28.5 ± 0.5 km s^{-1} and 70 ± 1 km s^{-1}, in good agreement with previous estimates of Strassmeier et al. (1999).

The rotation period (or the rotation law in the case of a differentially rotating surface) can be estimated in a similar way as v_{rad}, but

we leave the detailed analysis of surface differential rotation for Section 4. All the images presented hereafter are computed assuming that the surface undergoes differential rotation during data collection. We assume in the reconstruction process a surface rotation law of the type:

$$\Omega(l) = \Omega_{\rm eq} - {\rm d}\Omega \sin^2 l \quad (1)$$

where $\Omega(l)$ is the rotation rate at latitude l, $\Omega_{\rm eq}$ the rotation rate of the equator (set to 1.934 rad d^{-1}, see Section 4) and dΩ the difference in rotation rate between the pole and the equator (set to 66 mrad d^{-1} by default). We assume a mean rotation period equal to 3.3 d (1.904 rad d^{-1}) for calculating the rotational phases. Given the differential rotation parameters assumed for the star, this period is the one we expect at latitude 42° (rotation periods of the stellar surface varying from 3.25 d at the equator to 3.36 d in the polar region). The adopted ephemeris is:

$$\mathrm{JD} = 2451150.675 + 3.3\phi \quad (2)$$

where ϕ is the rotational phase and JD the Julian date. Considering this 3.3 ± 0.05 d rotation period and using the v sin i value derived above, we estimate the stellar radius to be R sin i = (4.5 ± 0.1) R$_\odot$. This value is compatible with a previous estimate of Hackman et al. (2001, based on *Hipparcos* parallax measurements) that yields a stellar radius of 4 R$_\odot$< R < 5 R$_\odot$). However, high values of i are obviously required to stay consistent with the *Hipparcos* radius. Considering several Doppler images reconstructed with different values of the inclination, the highest possible value of i is about 50°, since higher inclination angles produce obviously spurious structures on the images. For this inclination the value of the stellar radius is roughly 5.8 R$_\odot$, higher than that proposed by Hackman et al. However, as emphasized by these authors and by Strassmeier et al. (1999), the *Hipparcos*-based estimate critically depends on the physical models used to describe such a post-main-sequence star. Given the rather unusual physical properties of HD 199178 (among which its high rotation rate and its uncertain evolution on the main sequence, since this single star may come from the coalescence of a close binary system), this kind of discrepancy is not surprising, therefore we choose to use our estimate $i = 50°$.

To summarize, stellar parameters adopted in the imaging process are $i = 50°$, $v_{\rm rad} = -28.5$ km s^{-1}, v sin i = 70 km s^{-1}, $\Omega_{\rm eq}$ = 1.934 rad d^{-1} and dΩ = 66 mrad d^{-1}.

3 RECONSTRUCTED IMAGES

Nine brightness and eight magnetic images were reconstructed from the data sets described in Section 2, corresponding to epochs 1999.02, 2001.54, 2001.97, 2002.46, 2002.50, 2002.56, 2003.51, 2003.55 and 2003.58 (Figs 1–9). The early observations of 1998 December provided the first detection of a magnetic field on HD 199178. Several images were reconstructed from subsets of the large data sets secured in the summers of 2002 and 2003, to take into account the short-term variability of the photosphere occurring during data collection (see the discussion of this point in Section 3.3).

Owing to the relatively low S/N of the 2001.54 data set (3600 in average in Stokes V, i.e. 40 per cent below the mean S/N level of epoch 1999.02 for instance), none of the polarized profiles secured in this epoch provide a magnetic field detection, thus only a brightness image was constructed (Fig. 2). All the surface topologies described hereafter are reconstructed with a reduced χ^2 (hereafter $\chi^2_{\rm r}$) of 0.65 and 0.9 for brightness and magnetic images, respectively. A $\chi^2_{\rm r}$ smaller than unity is adopted to take into account the fact that error bars derived from MuSiCoS observations are slightly overestimated (Wade et al. 2000).

3.1 Brightness surface structures

The most obvious characteristic of the brightness topology of HD 199178 is the presence of a large polar spot in all images. This cool region is always quasi-axisymmetric and covers most of the stellar photosphere above latitude 60°. At several epochs, the polar spot is partly fragmented, with smaller spots clearly distinguishable from the main polar component (e.g. at epoch 1999.02, when a smaller, secondary spot was visible at phase 0.0 and latitude 80°).

In addition to the polar spot, smaller spots appear at lower latitude, but only about 5 per cent of the overall spot coverage is contained within the low-latitude features (below latitude 30°). The latitudinal spot distribution is rather stable from one epoch to the next (see Fig. 10 for epoch 2002.50) and repeatedly presents a peak of spot occupancy between latitudes 15° and 30°, with a relative gap of spottedness in regions next to the equator and within a band extending from latitude 30° to the outer limit of the large polar cap.

In Fig. 11 we plot the latitudinally averaged spot coverage, as a function of the rotational phase, for each subset of the summer of 2002 (left panel) and the summer of 2003 (right panel). The first information provided by these curves is that the observed spot distribution varies greatly between subsets that are near in time. Part of this apparent evolution can be explained by the different phase sampling achieved for different subsets, producing a lack of signal at some longitudes. However, if phase gaps can be a problem at some epochs (e.g. 2002.46), most of the subsets possess good phase sampling, particularly in 2003. In order to obtain a more precise estimate of potential biases due to phase gaps, we compare successive subsets secured at close-by epochs with a different phase sampling (but bearing in mind, however, that short-term evolution of the spot distribution also accounts for part of the observed differences, see Section 3.3).

The spot coverage was marginally higher in 2002 on phases ranging from 0.25 to 0.65 (with two distinct maxima of spot coverage visible around phases 0.35 and 0.55). In 2003, the maximum spottedness is rather concentrated between phases 0.8 and 0.2. In 2002, longitudes with the largest filling factor are clearly linked to the presence of low-latitude spots (see Figs 4–6), while in 2003 features spatially associated to the large polar cap are mostly responsible for the higher spottedness around phase 0.0. For other epochs, the biases due to uneven phase coverage cannot be as accurately estimated as for the 2002 and 2003 data sets. However, if the phase sampling is far from optimal at epochs 1999.02 and 2001.54, there is no significant phase gap at epoch 2001.97, for which we note a maximum spot coverage around phase 0.9 (corresponding plot not shown here).

3.2 Magnetic topology

The magnetic topology of HD 199178 features several regions of intense field strength (in excess of 1 kG). Owing to the fact that polarized profiles used here suffer from a relatively high noise level (compared to previous studies of active stars based on ZDI), the constraints provided on the magnetic maps are not very high, so that several assumptions on the field are compatible with an image reconstruction at a fixed $\chi^2_{\rm r}$ (equal to 0.9). For instance, the maps can be calculated assuming either a purely radial field or a mixture of all three possible components of the field (radial, azimuthal and

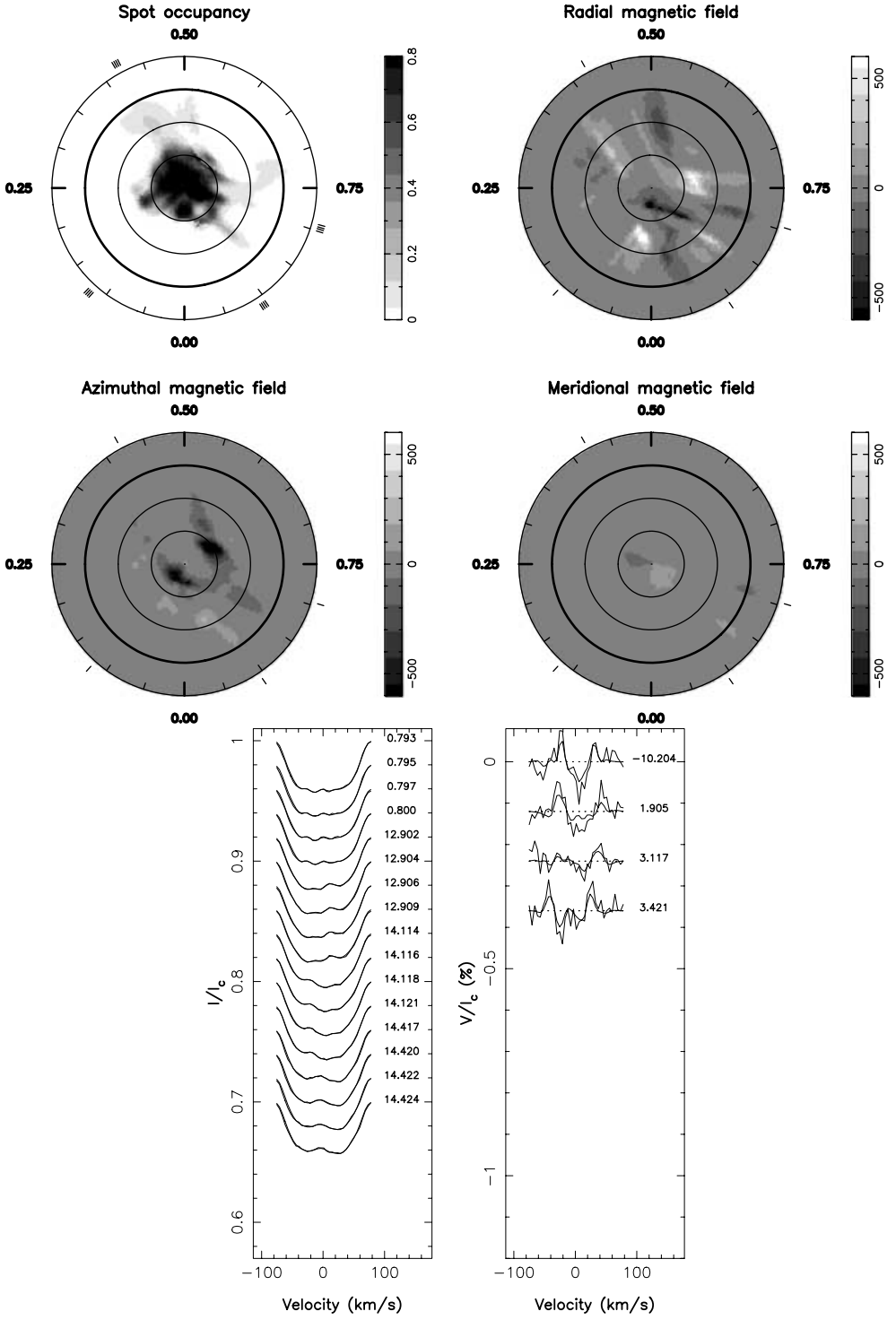

Figure 1. Reconstructed images of HD 199178 at epoch 1999.02, in flattened polar view. The concentric circles correspond (starting from the outside) to parallels of latitude −30°, 0° (equator, bold line), +30° and +60°. The upper-left panel corresponds to a brightness image, while the three other charts show the components of the magnetic field (in Gauss) in spherical coordinates, i.e. radial, azimuthal and meridional components of the field in the upper-right, lower-left and lower-right charts, respectively. Stokes I and V normalized profiles are plotted in the lower part of the figure (left-hand panel and right-hand panel, respectively). Thin lines represent the observed profiles, while bold lines correspond to profiles reconstructed by the imaging code.

meridional). To select between these two possibilities, the very principle of maximum entropy imaging tells us that the image exhibiting the lowest information content is the most likely (the information contained in the map being calculated as the integrated field strength over the stellar surface, hereafter $B_{\rm mod}$). Taking epoch 2003.58 as an example, a purely radial photospheric field leads to $B_{\rm mod} = 74$ G. For the same data set, $B_{\rm mod}$ is equal to 46 G for an image containing all three components of the field. Very similar results can be derived

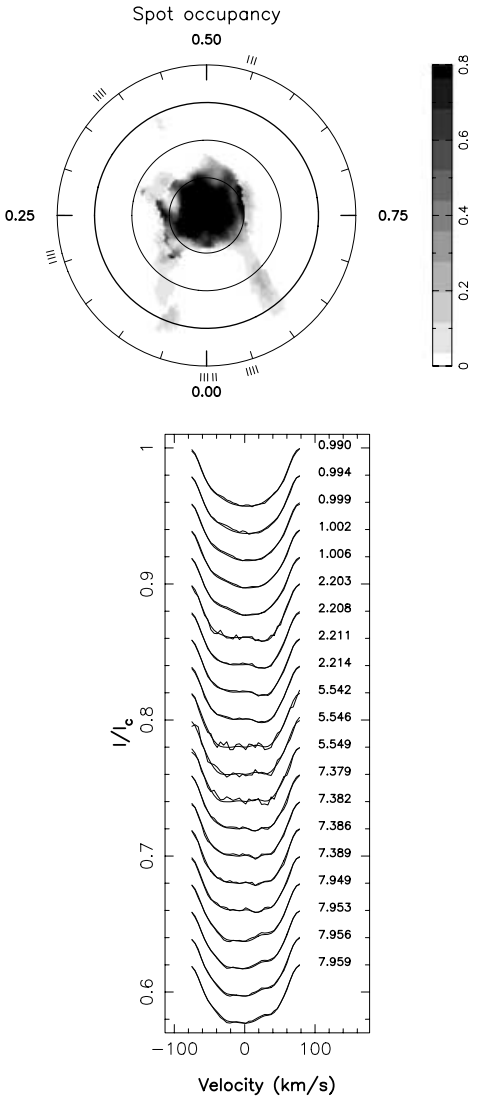

Figure 2. Same as Fig. 1 for the 2001.54 data set. There was no Zeeman signature detected at this epoch, owing to the high noise level of Stokes V profiles (see Table 1).

for all other epochs, with $B_{\rm mod}$ about 30–60 per cent higher for a purely radial field than for the map containing all three field components. At this stage, it can be argued that assuming the presence of an azimuthal component is not absolutely necessary for computing the magnetic maps. However, several additional reasons lead us to consider this component as genuine, as detailed below and in Section 5.

The reconstructed azimuthal field component can itself be divided into a couple of subcomponents of opposite polarities, with a predominance of clockwise field at high latitude, the lower latitudes being dominated by a counter-clockwise magnetic field. The left panel of Fig. 12 shows the longitudinally integrated distribution of the azimuthal field (averaged over all observing epochs). Both subcomponents can be clearly distinguished, with the field polarity changing sign around latitude 50°. The fact that the azimuthal component presents a consistent large-scale geometry between different images (despite very different S/N or phase coverage) suggests that the observed structures cannot be attributed to a problem of data quality (like noise or phase covering).

The clockwise subcomponent shows up in all images. At epoch 2001.97 for instance, a succession of several blobs of intense field strength draws the outline of a ring encircling the pole at the outer border of the cool polar spot. We also see an almost complete ring at epochs 2003.55 and 2003.58, whereas images reconstructed at other observing periods feature only a few spots of clockwise field, most of the time coincident with the edge of the polar spot. At some epochs (e.g. 2003.58), it can be noticed that spots belonging to the clockwise subcomponent show up within the dark polar cap, whereas we expect very few polarization signatures from this region because of the important brightness contrast with the unspotted photosphere (at a fixed field strength, Zeeman signatures formed inside the polar cap will be much fainter than that formed in the surrounding photosphere). Some of these structures may indeed belong to the outer region of the polar spot, but reconstruction biases of the imaging code can slightly shift these magnetic regions toward higher latitudes (Petit et al. 2002). It cannot be excluded, however, that we observe Zeeman signatures formed inside the polar spot. In this case, the reconstructed magnetic field must be considered with caution, since the field strength is likely underestimated.

The counter-clockwise component of the azimuthal magnetic field appears more discreetly between latitudes 10° and 40°. At epoch 2003.58, for instance, several spots of azimuthal field appear around latitude 40°, but with a relatively low field strength (reaching about 0.6 kG at phases 0.5 and 0.9). The low level of the magnetic flux emerging from these regions (Fig. 12) explains why such components cannot (or only marginally) be reconstructed at epochs for which the data suffer from a lower S/N (epochs 2002.50 and 2002.56 for instance).

In addition to areas hosting an azimuthal magnetic field, we reconstruct several regions in which the field is mostly radially oriented. On most images, the radial field is organized in an intricate pattern mixing opposite polarities, with a large-scale structure much less obvious than that of the azimuthal component. We note also that the radial field regions vary a lot between images corresponding to close-by epochs, which may lead us to question their reality. Numerical simulations indeed suggest that the noise pattern is preferentially reconstructed as radial field regions (but this effect is expected to be significant only for S/N much lower than that achieved here). As a test, we divide all the epoch 2003.58 data into two independent data sets by taking the odd numbered spectra to generate one image and the even numbered spectra to generate a second image (both images not shown here). The smallest radial field regions obtained in the corresponding images show little similarities between both maps, while all larger structures are coherently reconstructed. We emphasize, however, that reconstructing a map with one half of the profiles is tantamount to increasing the noise by a factor $\sqrt{2}$. Given the fact that the reconstructed magnetic distribution is therefore less accurate, we caution that discrepancies at small scales in the radial field pattern do not demonstrate that small-scale structures are not reliable in images better constrained. Furthermore, the good consistency achieved for all large structures is a good indicator of their reality.

The largest radial field regions are observed at epochs 2002.46 and 2003.58, when two large unipolar areas are seen close to the pole. Contrary to the azimuthal field, no latitudinal organization of the radial field can be readily seen on the different images. However, if we average the radial field component over all observing epochs (Fig. 12), we note that a positive field dominates at high latitude, while regions presenting a negative polarity are mostly confined below latitude 40°. Despite this statistical trend, it can be seen on some images that a negative polarity can sometimes dominate the

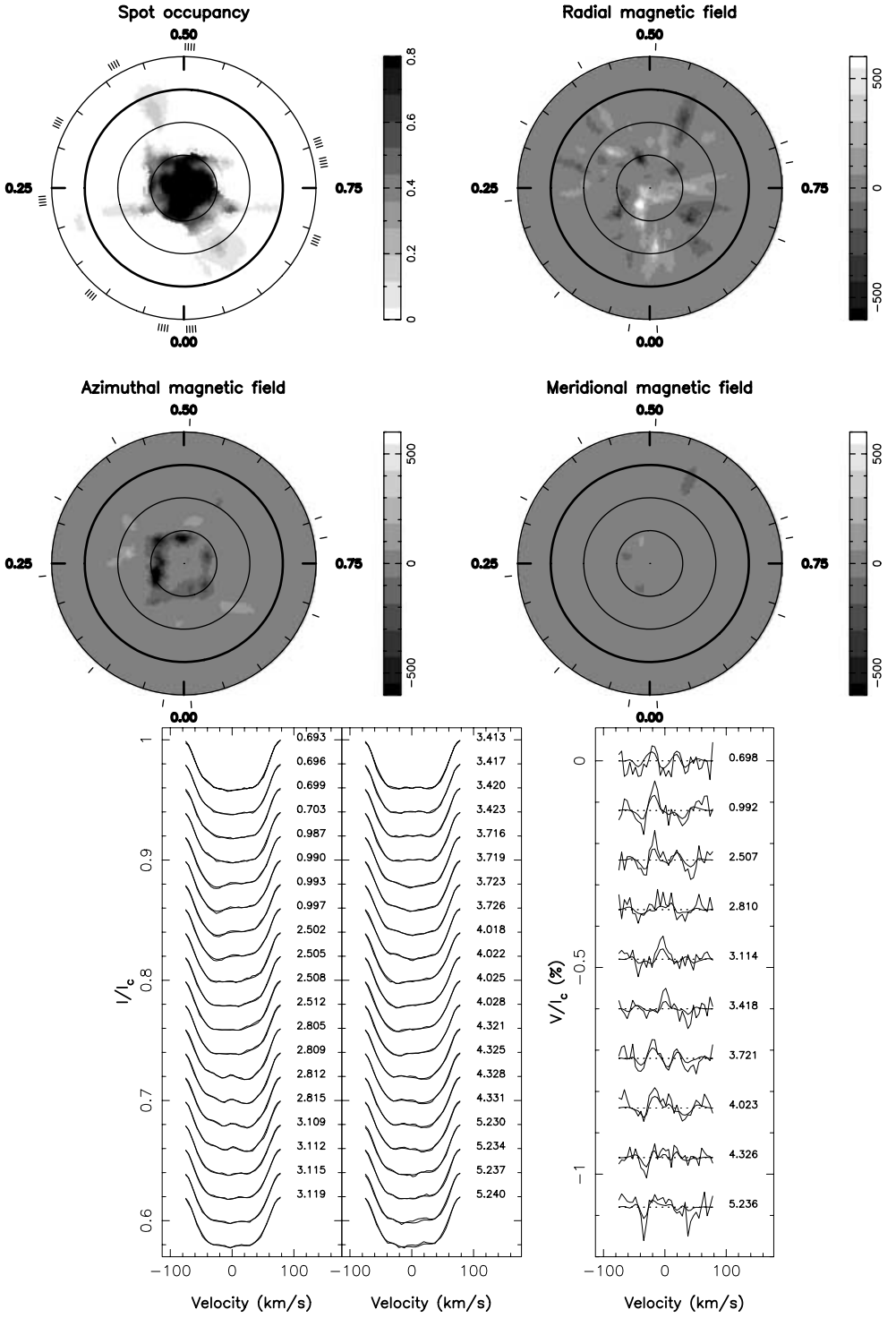

Figure 3. Same as Fig. 1 for the 2001.97 data set.

radial component at high latitude (at epochs 1999.02 and 2002.56 for instance).

A small part of the polar magnetic field is sometimes reconstructed as a meridional field component (see, e.g. Fig. 5). These high-latitude azimuthal and meridional features indeed belong to the same physical structure (a region containing mostly horizontal field and located over the pole), an effect (detailed by Donati 1999) that can be attributed to the singular nature of the pole in spherical coordinates. Other structures appearing in the meridional field component at lower latitude (see, e.g. very faint structures around phase 0.5 at epoch 2003.58) can be partly produced by known reconstruction cross-talk between radial and meridional fields (Donati & Brown 1997), an effect essentially negligible in the case of HD 199178 thanks to its relatively high inclination angle.

The radial magnetic field is always the main contributor to the photospheric magnetic energy (at roughly 85 per cent of the overall

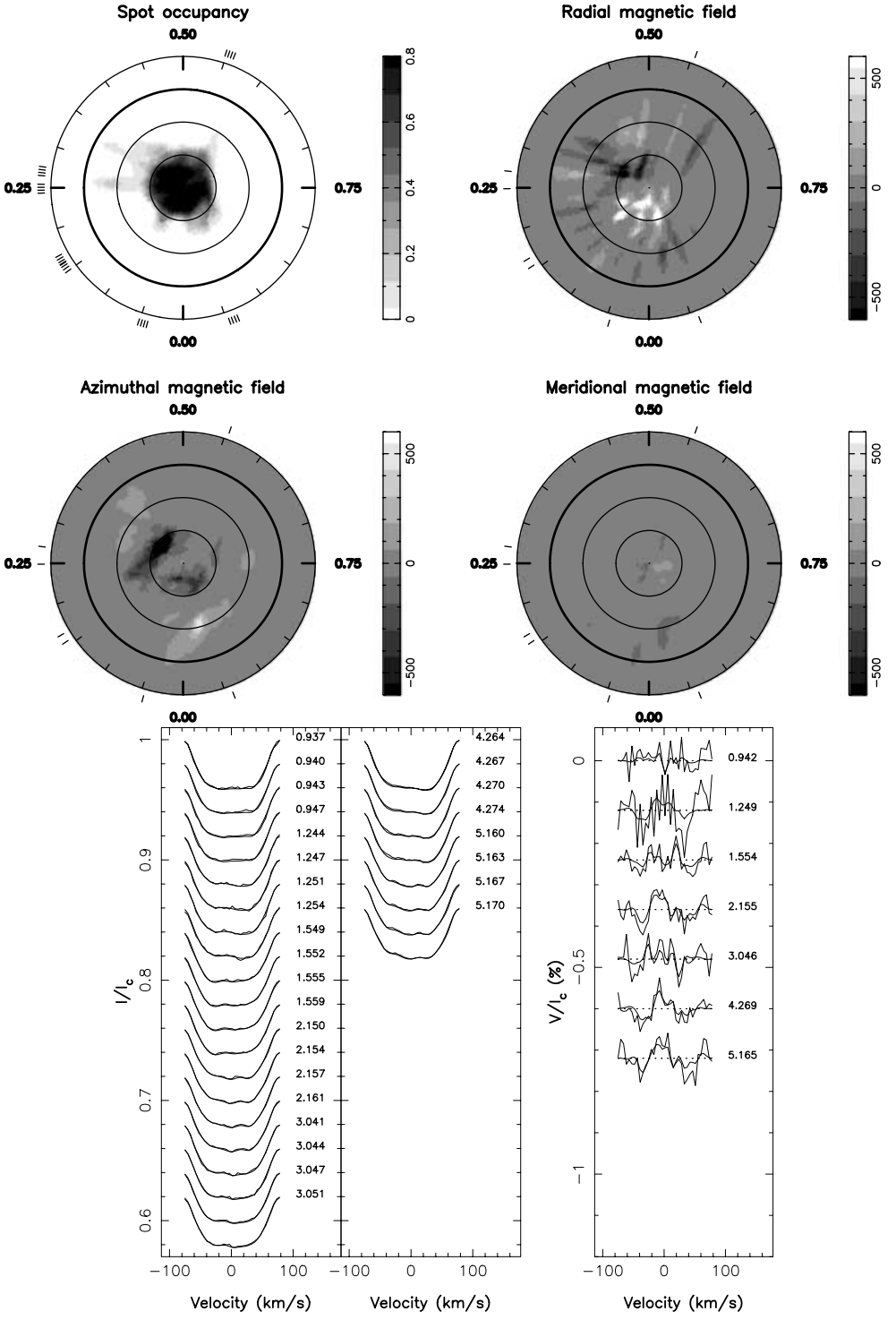

Figure 4. Same as Fig. 1 for the 2002.46 data set.

energy). However, numerical simulations suggest that this fraction is sensitive to the S/N and may become important for low-quality data (part of the noise producing radial field structures, even for very slight overfitting of the data). In order to avoid this problem, a solution consists in calculating the energy stored in the longitudinally integrated field. By doing so, we average out most of the noise, but we also ignore most of the energy contained in small-scale magnetic regions. It is, however, an opportunity to estimate the energy stored within the large-scale axisymmetric field, which is otherwise partly hidden among small magnetic features. We find that the radial field contributes only to some 10 per cent of the global energy contained in the large-scale field (at epochs 2001.97 and following), which means in other words that the axisymmetric field is largely dominated by its azimuthal component.

At epochs 2002.46, 2002.50 and 2002.56, the low-latitude ring of azimuthal field constantly contains about 14 per cent of the

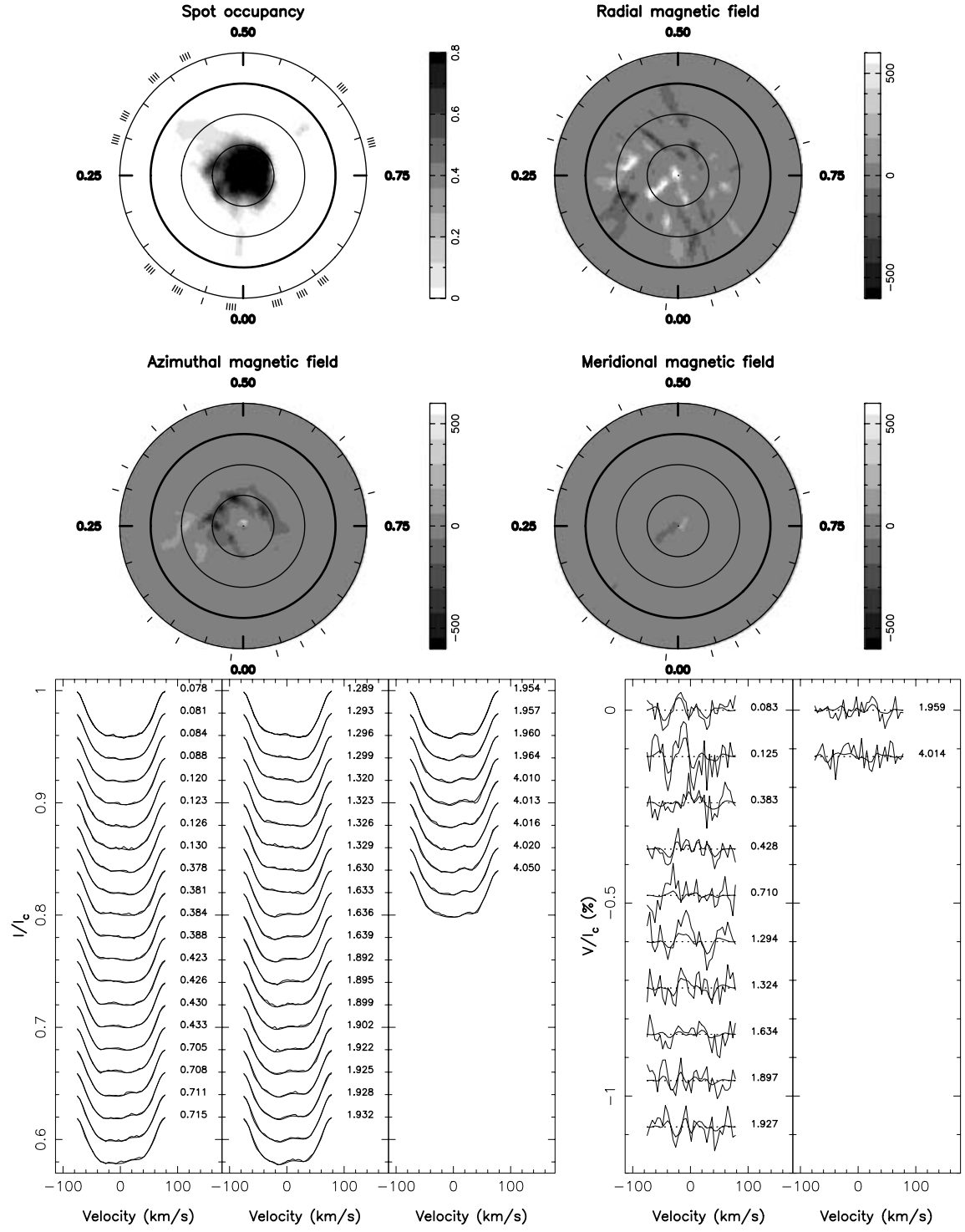

Figure 5. Same as Fig. 1 for the 2002.50 data set.

total amount of energy stored within the azimuthal component of the axisymmetric field. This fraction is stable despite large variations of the S/N and phase coverage over the three corresponding data sets, suggesting that data quality only marginally impacts this estimate. The fraction was equal to 6 per cent six months earlier at epoch 2001.97 (with significantly better S/N and comparable level of phase coverage) and reaches about 20 per cent between 2003.51 and 2003.58. We suggest that this evolution may be genuine, with respective weights of both azimuthal field rings remaining rather stable over a few weeks, but showing significant evolution on timescales ranging from a few months to several years.

The latitudinally averaged distribution of the photospheric field as a function of the rotational phase is plotted in Fig. 13 for data sets secured during the summers of 2002 and 2003. A larger magnetic flux is observed between phases 0.2 and 0.4 during the summer of 2002, but with significant differences between the three curves

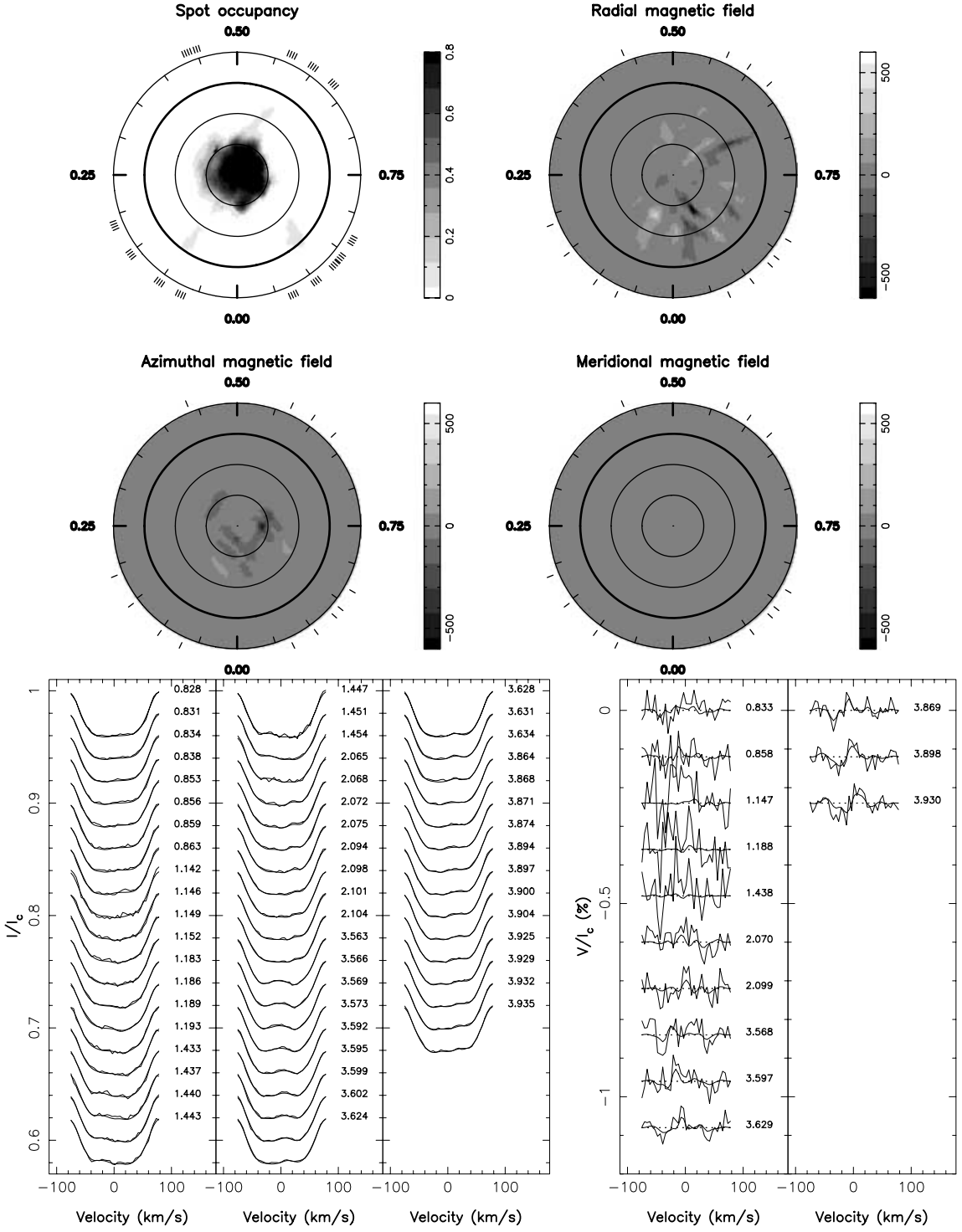

Figure 6. Same as Fig. 1 for the 2002.56 data set.

corresponding to epochs 2002.46, 2002.50 and 2002.56. We will discuss in Section 3.3 whether short-term evolution of active regions can account for this apparent discrepancy. At epoch 2002.56 and during the summer of 2003, the distribution of the magnetic flux is mostly independent of the rotational phase. In particular there is no apparent correlation between the phase distributions of cool-spots (Fig. 11) and magnetic field.

3.3 Rapid surface changes

During the summers of 2002 and 2003, HD 199178 was observed every clear night, thus providing a monitoring (over two distinct periods covering about 45 d) of the evolution of surface structures.

The intrinsic evolution of the photosphere is first obvious in the profiles themselves. For instance, striking differences are visible

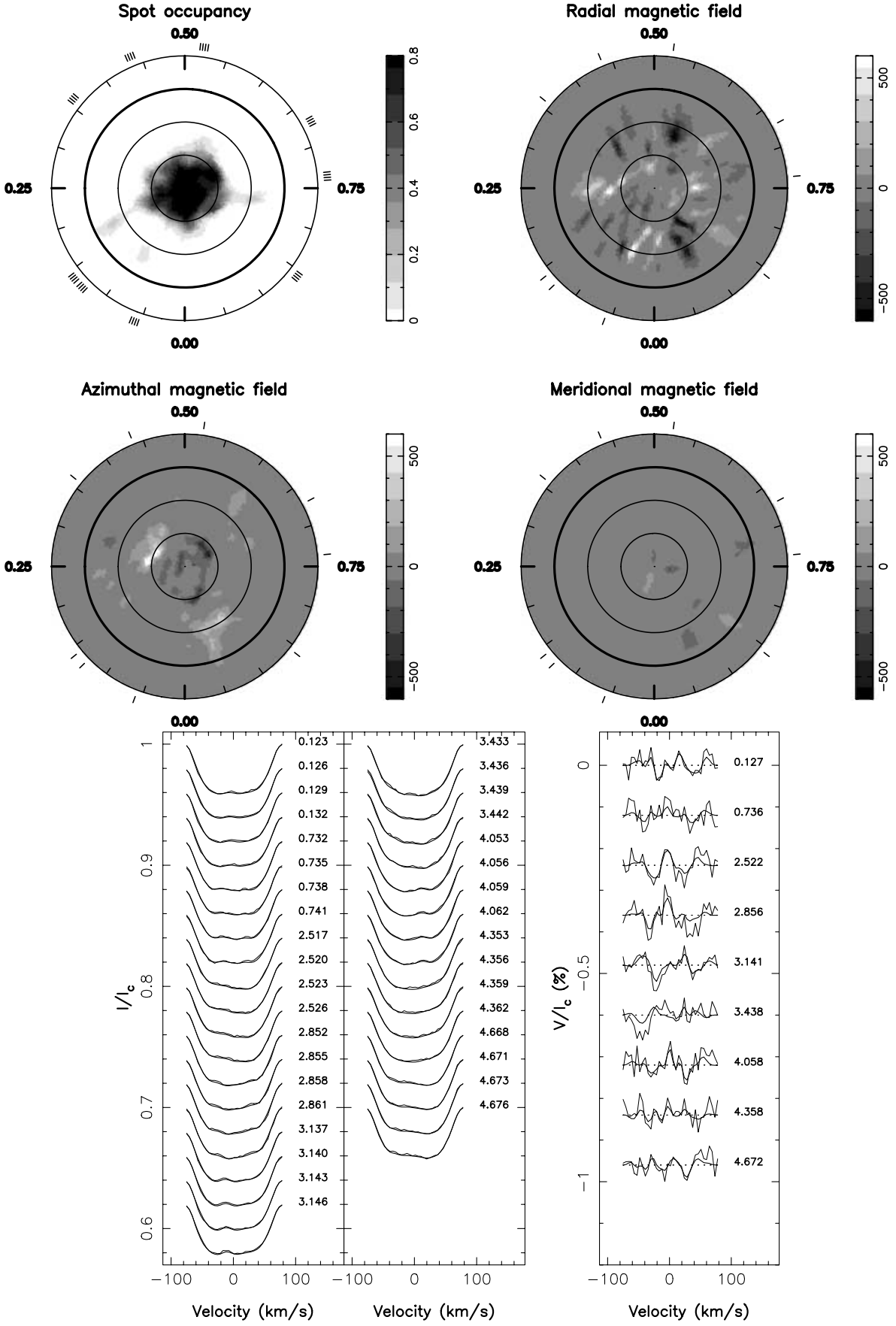

Figure 7. Same as Fig. 1 for the 2003.51 data set.

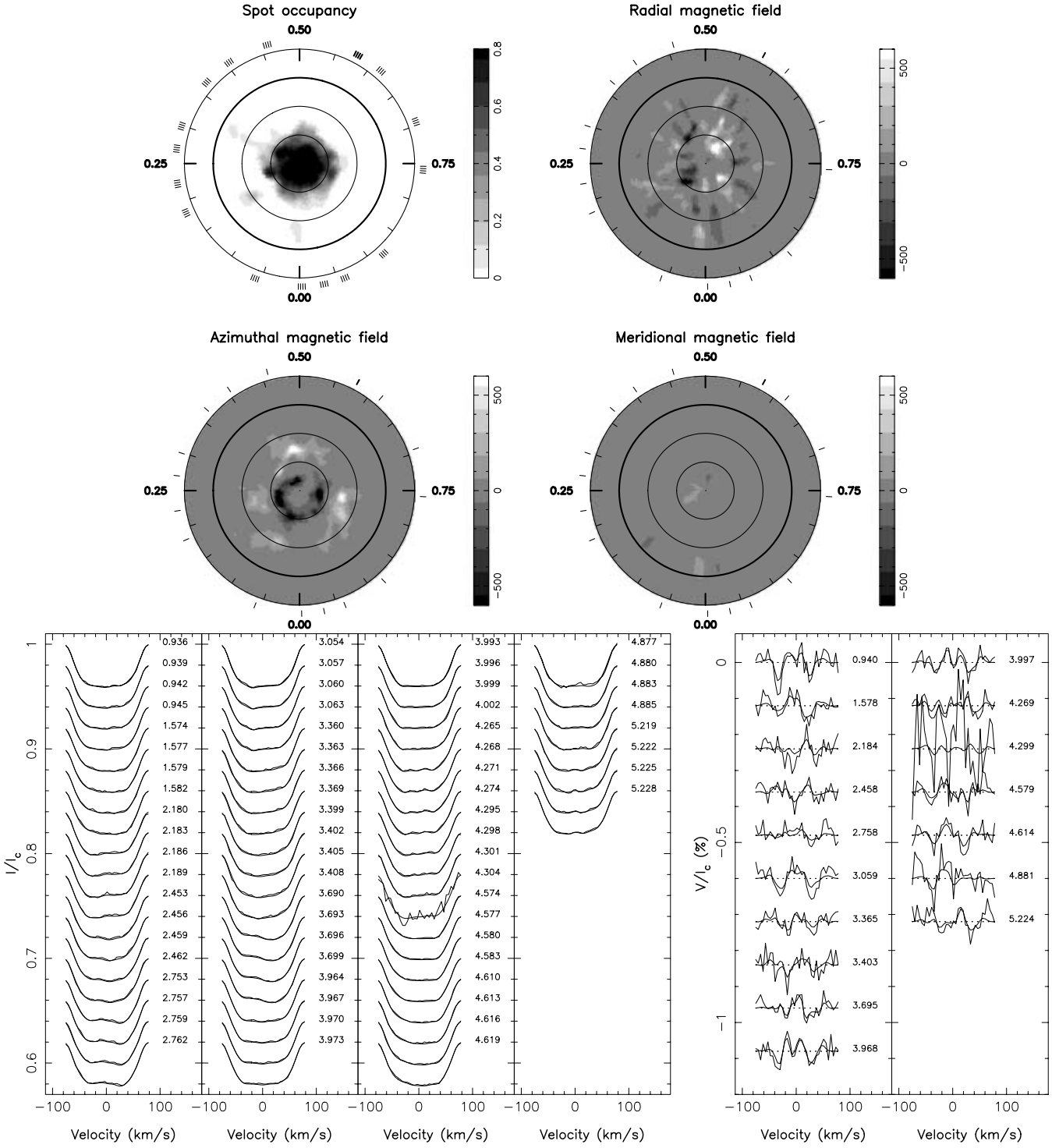

Figure 8. Same as Fig. 1 for the 2003.55 data set.

between the brightness profiles secured on 2002 June 13 and 2002 July 26, i.e. 43 d apart (Fig. 14), despite a difference in rotational phase as small as 0.4 per cent of a rotation cycle. In this specific case, the wide bump appearing at the centre of the most recent profile has no equivalent 6 weeks before.

The second piece of evidence for surface variability arises from a monitoring of the χ^2_r of the reconstructed images. When grouping the data secured from 2002 June 28 to 2002 July 28 in a single data set (i.e. grouping epochs 2002.50 and 2002.56), we cannot reconstruct surface images with a χ^2_r lower than 0.85 and 1 for the brightness and magnetic images, respectively, as opposed to a χ^2_r of 0.65 and 0.9 when reconstructing separate images from each subset. To ensure that the data sets employed to produce the surface images do not spread on too long a time-span, we split the global data sets of the summers of 2002 and 2003 into successive subsets corresponding to epochs 2002.46, 2002.50, 2002.56, 2003.51, 2003.55 and 2003.58

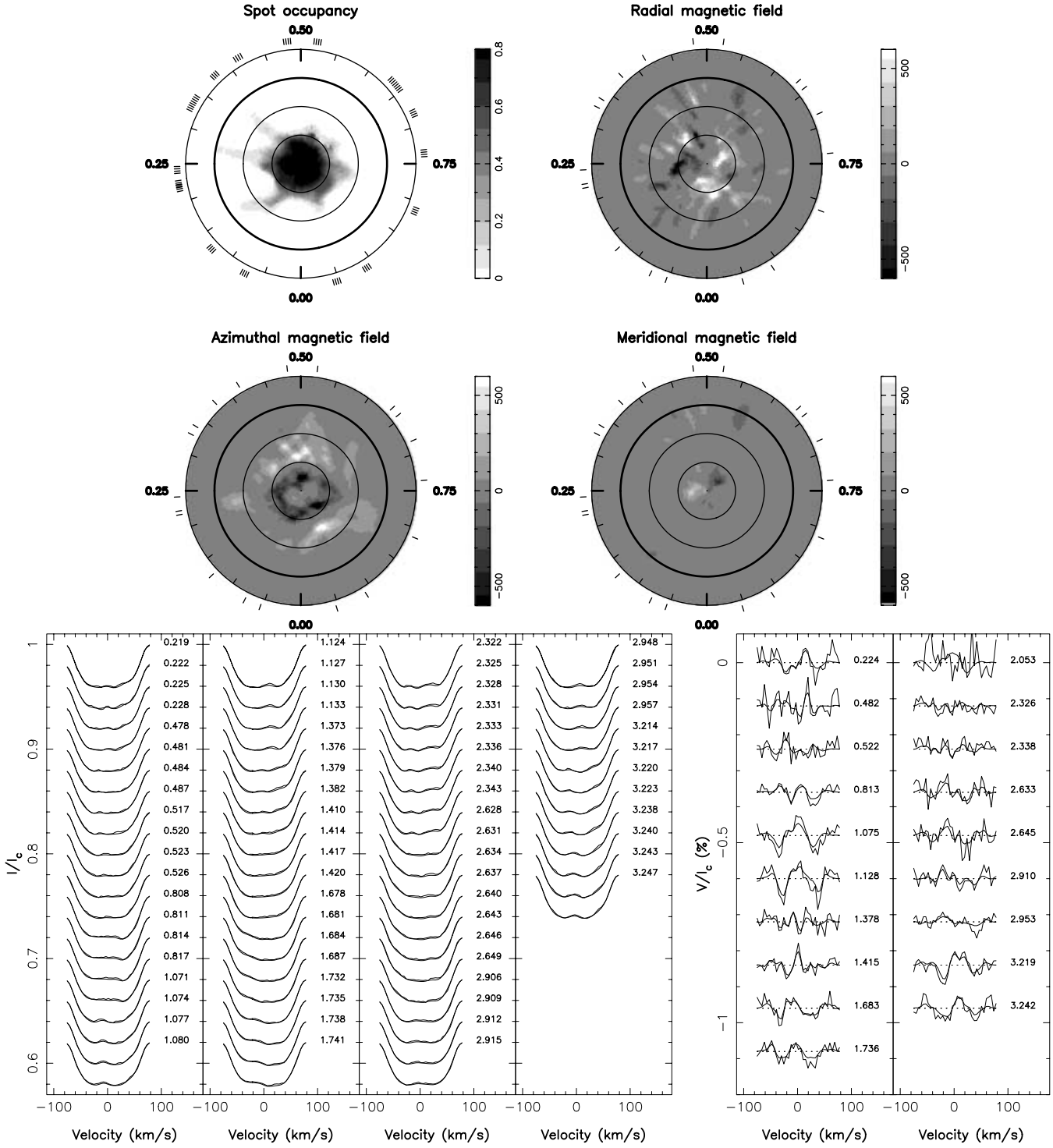

Figure 9. Same as Fig. 1 for the 2003.58 data set.

(respectively covering 14, 13, 11, 15, 13 and 11 nights). We then use this time series to get a direct view of the surface evolution of brightness and magnetic structures. In the following paragraphs, we voluntarily limit the comparisons between pairs of images to high-latitude structures and to the low-latitude regions located at rotational phases observed in both data sets, in an attempt to avoid as much as possible differences produced by reconstruction biases associated to phase gaps.

Considering the set of brightness images, we first note the continuous birth and disappearance of low-latitude spots. For instance, the spot located at phase 0.4 and latitude 70° at epoch 2003.58 cannot be associated to any structure observed at epochs 2003.51 and 2003.55. On the other hand, the spot reconstructed around phase 0.17 and latitude 25° at epochs 2003.51 remains clearly visible until 2003.58 (small changes in its exact location and shape from one epoch to the next being compatible with usual reconstruction biases).

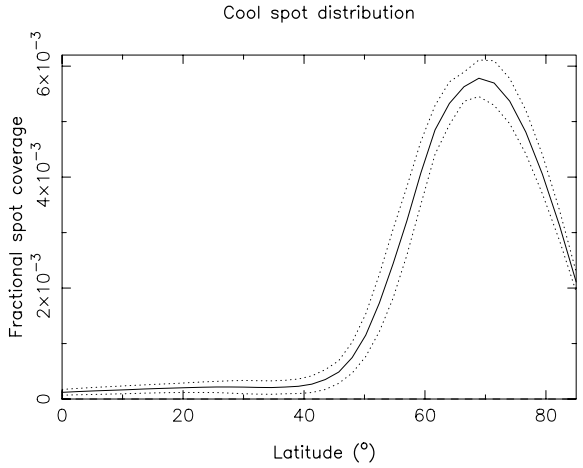

Figure 10. Distribution of the fractional spot coverage as a function of latitude. The solid curve represents the flux averaged over all observing periods. The two dotted curves surrounding the mean curve show the standard deviation.

Rapid changes also affect brightness inhomogeneities at the limit of the polar spot during similar time-scales. The edges of the polar cap (from phases 0.0 to 0.5) are rapidly evolving during the summer of 2002, with two secondary spots appearing next to the main component of the polar spot between epochs 2002.46 and 2002.50, then followed by a third region, located around phase 0.98 at epoch 2002.56. Note that these small spots are located around latitude 60° and therefore are sufficiently far from the pole to produce significant rotational modulation in the spectra. Considering also that these structures are never eclipsed during stellar rotation, we can conclude that the location of such cool-spots is very well constrained, so that the evolution we report here is very likely to be real.

The same type of evolution is observed for magnetic regions, with striking changes in the magnetic topology occurring on time-scales as short as a couple of weeks. One of the most obvious changes concerns the large azimuthal field region located at phase 0.5 and latitude 45° at epochs 2003.55 and 2003.58, which has no counterpart at epoch 2003.51. Another striking example concerns the very intense, large spot located at phase 0.4 and latitude 60° at epoch 2002.46. The field strength inside this region, in excess of 1 kG at epoch 2002.46, rapidly decreases to about 100 G in epoch 2002.56 (this evolution explains part of the differences between curves plotted in the left panel of Fig. 13). We caution, however, that the relatively low S/N of data sets corresponding to epochs 2002.50 and 2002.56 may also be partly responsible for the observed evolution.

Concerning the spots of radially oriented magnetic field, only the largest structures seem to possess lifetimes longer than a couple of weeks. As an illustration, the large region of positive field located near the pole at epoch 2002.46, which has already partly disappeared at epoch 2002.50, is then replaced by a region of opposite polarity at epoch 2002.56. We must nevertheless keep in mind that the location and field strength of magnetic regions inside the dark polar spot are likely to be affected by reconstructions biases, as already outlined in Section 3.2.

4 DIFFERENTIAL ROTATION

In this section, we study the motion of surface structures under the effect of differential rotation, applying the dedicated method of Petit et al. (2002) and assuming a surface rotation law similar to that given by equation (1). Considering a time series of profiles, up to 2000 images are computed (either brightness or magnetic maps, depending whether polarized or unpolarized profiles are considered) assuming different values of the differential rotation parameters $\Omega_{\rm eq}$ and $\mathrm{d}\Omega$ and imposing a constant information content in all images. In the case where the data quality is good enough, the reconstructed images present a $\chi^2_{\rm r}$ minimum corresponding to the most likely set of differential rotation parameters. Considering a $\chi^2_{\rm r}$ map obtained from the whole set of computed images (e.g. Fig. 15), the region around the $\chi^2_{\rm r}$ minimum can be approximated by a paraboloid, whose radius of curvature around its minimum gives the formal error bars on both parameters $\Omega_{\rm eq}$ and $\mathrm{d}\Omega$ (Donati et al. 2003b).

Only three of our data sets provided a detection of differential rotation (Table 3). The first one corresponds to observations obtained at epoch 2001.97. The two others are subsets taken from the large

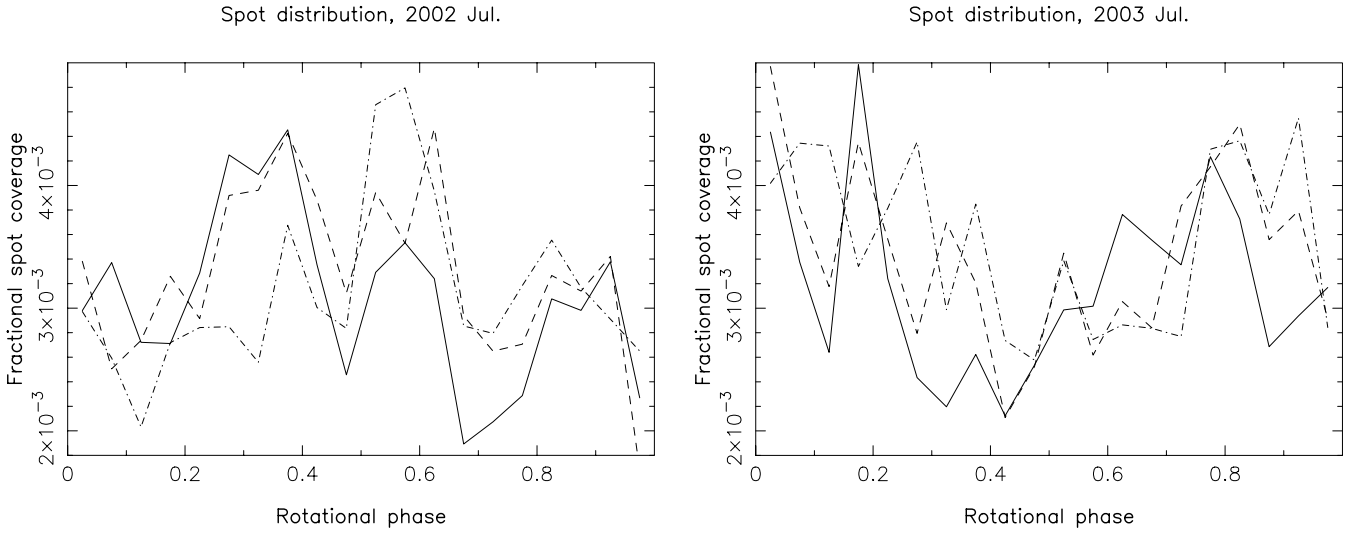

Figure 11. Distribution of the fractional spot coverage as a function of the rotational phase in 2002 and 2003 (left-hand and right-hand panels, respectively). Individual curves are derived from successive data subsets (2002.46 and 2003.51 in full line, 2002.50 and 2003.55 in dashed line, 2002.56 and 2003.58 in dot-dashes).

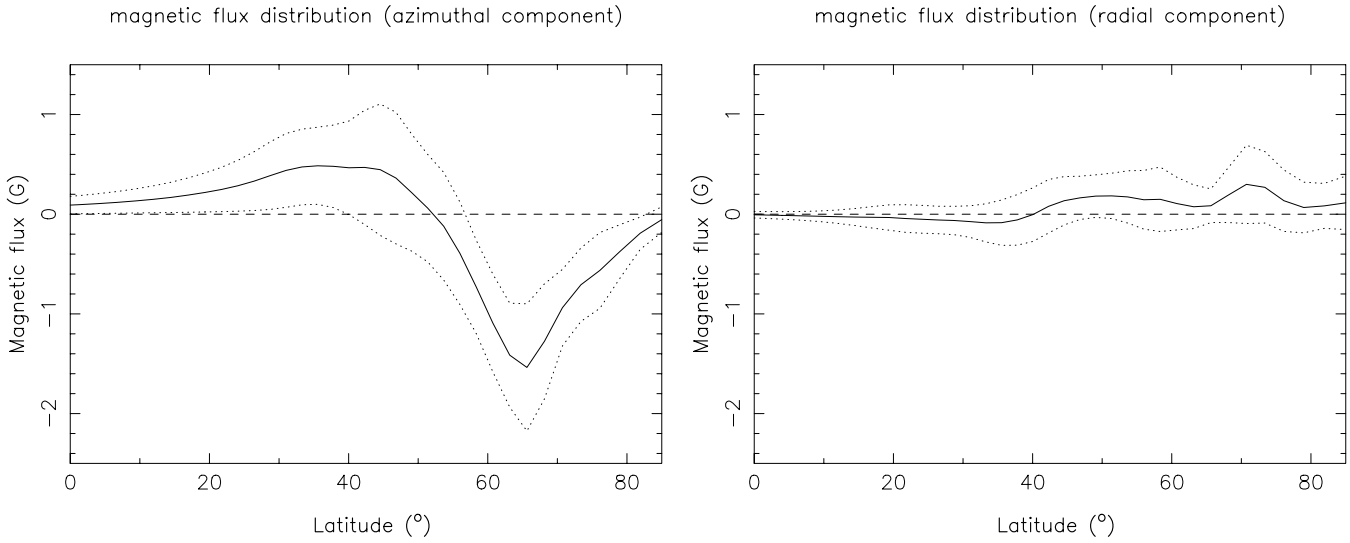

Figure 12. Latitudinal distribution of the azimuthal (left) and radial (right) components of HD 199178 magnetic flux. The full-line curves represent the flux averaged over all observing periods. The dotted curves show the standard deviation.

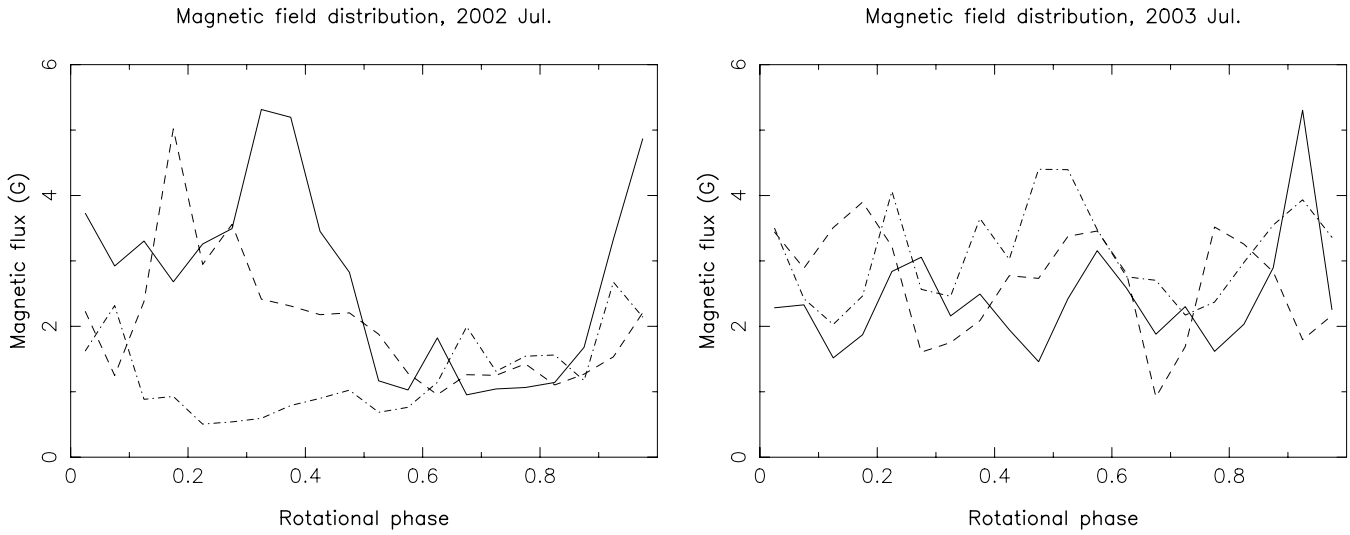

Figure 13. Same as Fig. 11 for the fractional magnetic flux.

data sets of the summers of 2002 and 2003. In the summer of 2002, we consider profiles secured between June 15 and July 2. In the summer of 2003, the subset is built from observations ranging from July 21 to August 5. Subsets of 2002 and 2003 observations are chosen to present the best compromise between phase sampling, noise level and time-span. In particular, we ensure that the time-length of all data sets used to derive the differential rotation parameters is consistent with the typical time-scale of local changes in the photospheric structures, as discussed in Section 3.3. Measurements of the $d\Omega$ parameter give similar results in 2001.97 and 2003.57, with $d\Omega$ equal to 66 ± 28 mrad d^{-1} and 86 ± 20 mrad d^{-1}, respectively, indicating the detection of a solar-like differential rotation (the equator rotating faster than the pole) to within 4.3σ. The third estimate, corresponding to epoch 2002.48, suffers from error bars 2–3 times larger, but stays consistent with measurements from the other two epochs.

No other data set constituted of Stokes V profiles could provide a detection of differential rotation (no paraboloid shape of the χ^2_r map around χ^2_r minimum). A higher noise level, sparser phase sampling or local evolution of the distribution of magnetic regions during data collection may be responsible for this failure. We also note that no detection was achieved using Stokes I profiles. This is not a surprise, since cool-spots are mostly concentrated close to the pole on HD 199178, few tracers being available at lower latitude. On the contrary, the magnetic topology offers tracers densely distributed over the stellar surface, therefore spanning a larger range of rotation periods and allowing easier detection of surface shear.

As outlined by Petit et al. (2002, 2004), measurements of differential rotation can be partly affected by biases arising from low data quality. Also problematic is the potential aliasing due to intrinsic evolution of the photosphere (a newborn active region can be mistaken for an older one that has vanished during data collection, leading to inadequate evaluations of the shear). However, it is highly unlikely that an aliasing problem occurs for the three data sets presented here, and even more unlikely that the produced bias could shift our estimate of differential rotation toward the same (spurious)

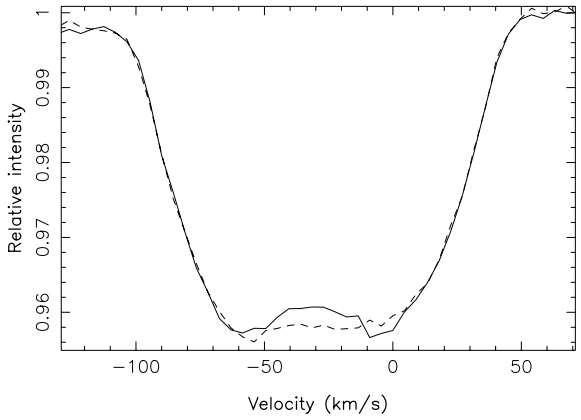

Figure 14. Stokes I profiles of HD 199178 obtained at phase 0.5588 on 2002 June 13 (dashed line), and at phase 0.5629 on July 26 (full line).

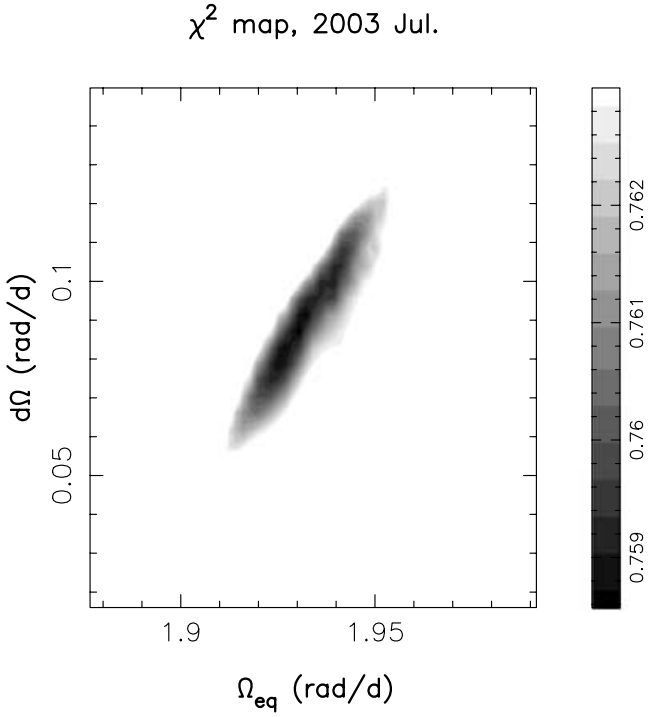

Figure 15. Reduced χ^2 map in the differential rotation parameter plane, obtained from polarized data of epoch 2003.57. Ω_{eq} is the rotation rate of the equator and dΩ the difference in rotation rate between the pole and the equator. The 1σ limit on the two parameters (considered separately) corresponds to the black region.

value. Given the fact that the data sets also present very different S/N and phase sampling, the three consistent measurements presented here suggest that the observed shear is genuine.

5 DISCUSSION

5.1 Brightness distribution

The magnetic activity of HD 199178 has been monitored by the present study over 4.5 yr. Several characteristics of its brightness topology remain constant during this whole period, the most obvious being a large axisymmetric polar spot reconstructed above latitude 60°. While dark polar caps are known to be a usual feature on Doppler images of fast rotators, their exact shape and evolution with time can significantly vary for different objects. The only other evolved star for which ZDI has been performed up to now (the K1 subgiant of the RS CVn system HR 1099, see, e.g. Petit et al. 2004) also possesses a cool polar region, but with a more complex shape and a fluctuating location of its centroid. Taking into account the regular, almost axisymmetric shape of the polar spot observed on HD 199178, Hackman et al. (2001) argue that the flat bottom of the photospheric Stokes I profiles (interpreted by imaging codes as a polar spot) may indeed be partly due to a distortion of line profiles under the effect of antisolar differential rotation (the polar region rotating faster than the equator). Our own measurements of the surface shear of HD 199178 suggest a solar-like differential rotation of magnetic structures, arguing against this possibility. Moreover, numerical simulations show that for shear intensities similar to those that we measure, line profile distortions do not exceed 10^{-4} of the continuum level, safely allowing us to assume that the differential rotation of HD 199178 does not produce significant biases in the imaging process.

Table 3. Surface differential rotation parameters derived for HD 199178, using Stokes V profiles. For each epoch, Ω_{eq} (equatorial rotation rate) and dΩ (difference of rotation rate between equator and pole) are listed.

Date year	Ω_{eq} rad d^{-1}	dΩ mrad d^{-1}
2001.97	1.934 ± 0.018	66 ± 28
2002.48	1.932 ± 0.033	79 ± 61
2003.57	1.931 ± 0.017	86 ± 20

5.2 Magnetic topology

The magnetic topology of HD 199178 presents at all observing epochs large regions in which field lines are mostly azimuthally oriented. Such magnetic regions have already been observed in several objects (e.g. Donati et al. 2003a) with sufficiently high S/N to erase any doubt about their reality. Here, two long-lived rings displaying opposite polarities are observed, encircling the pole at two distinct latitudes. The fact that we observe this large-scale structure on all maps suggests that it cannot be attributed to an artefact due to the noise pattern. This general configuration of the azimuthal field is very similar to that of HR 1099, whereas no such obvious axisymmetric structure has been reported for younger stars (which suggests that such large-scale characteristics of the magnetic topology are not a systematic bias produced by ZDI). The radial field component does not present a similarly axisymmetric structure.

This predominant azimuthal component may be connected to the toroidal component of the large-scale dynamo field, by analogy with dynamo models developed for the Sun. However, this would imply at the same time that the dynamo operating in HD 199178 is possibly different from that at work in the Sun. In the solar case, the toroidal field is believed to be mostly confined at the interface between the radiative core and the convective zone. The observation of this toroidal component at the photospheric level would therefore suggest that the dynamo of HD 199178 is active either very close to its surface, or maybe in its whole convective envelope. Steep subsurface velocity gradients are observed in the Sun (Corbard & Thompson 2002) and

it was investigated by Dikpati et al. (2002) whether a near-surface dynamo could be generated in this layer. They concluded, however, that such a mechanism could only marginally contribute to create a large-scale field. Recent simulations of Küker & Stix (2001), however, suggest that subsurface velocity gradients may be stronger for stars with deep convective zones and for fast rotators. In this context, the possibility that a subsurface dynamo may be efficient in a star like HD 199178 is an interesting option that could partly account for the observed strong azimuthal photospheric field.

5.3 Active longitudes

Recent studies (based on long-term photometric observations) report the presence of active longitudes on FK Com, a star very similar to HD 199178 (Korhonen et al. 2002). Furthermore, the same authors report occasional 180° shifts of the activity peak longitude, a phenomenon usually called 'flip-flop'. The kind of monitoring we propose in the present study is not adapted to analyse such an effect, due to an inadequate time interval between successive images (regular monitoring of HD 199178 over several months would be an appropriate observational basis in this aim). In our observations there is only marginal evidence that some rotational phases are more spotted than others (Fig. 11). It is also worth noticing that we do not detect any correlation between the phase distributions of spot coverage and magnetic flux (Fig. 13). This may suggest that the observed photospheric magnetic field is not directly connected to the internal field producing the cool-spot pattern. In particular, it gives further support to the idea that the observed magnetic structures may be formed close to the stellar surface, while cool-spots may reveal the action of a dynamo seated deeper in the stellar interior.

5.4 Magnetic cycle

The observed topology of the magnetic field is very stable over the whole observing period. While local modifications of the magnetic pattern occur on time-scales as short as a couple of weeks, some general characteristics of the large-scale field (like the rings of azimuthal field) only undergo marginal changes on the 4.5-yr observing window. Only two noticeable long-term changes can be reported here.

The first one is the progressive polarity reversal of the radial component of the field at high latitude, between epochs 2002.46 and 2002.56. No simultaneous variability of other large magnetic structures was noticed. A similar phenomenon was earlier reported for AB Dor (Donati et al. 2003a) but over a longer time-scale, of order of 1 yr. Even if we cannot exclude at this stage that this local evolution is part of the global activity cycle of HD 199178, the overall stability of the largest magnetic structures rather suggests that this kind of event is only local, thus not necessarily connected to a global variability of the large-scale field. The second noticeable evolution, which shows up on a time-scale of several years, is the increasing fraction of magnetic energy stored at low latitude in the azimuthal field component.

5.5 Surface differential rotation

We report the probable detection of a solar-like differential rotation on HD 199178, derived by a monitoring of the relative motion of surface magnetic tracers. The intensity of the surface shear, estimated from the difference in rotation rate between equatorial and polar regions, is roughly solar in magnitude, with a lap-time (time for the equator to lap the polar region by one complete cycle) equal to 80 days. The repeated detection of differential rotation from independent data sets and the size of the related error bars allows us to rule out the possibility of an antisolar differential rotation.

The fact that the shear intensity is similar in magnitude to that measured on several fast-rotating young dwarfs (Cameron 2002) may indicate that a difference in the depth of the convective zone has only a limited impact on the shear level. It was also suggested by Cameron considering a small sample of G and K active stars, that the lap-time may decrease for increasing stellar masses. With a mass slightly higher than that of other stars of this sample (a stellar mass of 1.65 $M_{\odot}$ was proposed by Hackman et al. 2001), the lap-time of HD 199178 is also among the shortest measured on other active G and K stars, therefore giving further support to this idea.

A very weak solar-like surface shear similar to that detected on HR 1099 (Petit et al. 2003, report for this star a lap-time equal to 480 d) is excluded to the 4σ level. Both HR 1099 and HD 199178 are evolved stars with deep convective envelopes, therefore we do not expect a difference in their evolutionary stage to be responsible for such a discrepancy. A possible explanation is that the strong tidal forces operating in the convective envelope of HR 1099 are responsible for its very weak differential rotation, though observations of other close binaries are obviously needed to confirm this result and disentangle the influence of a tidal torque from that of other stellar parameters.

The lifetime of surface structures, reported to undergo fast changes over periods as short as a couple of weeks, is similar to values suggested by earlier studies of young dwarfs (Barnes et al. 1998), but much shorter than on HR 1099 where typical active regions remain stable on time-scales as long as 4–6 weeks. The smaller size of most magnetic and spotted regions of HD 199178 may partly explain this difference in lifespan, as well as its stronger differential rotation producing a more intense shear of active regions.

6 CONCLUSIONS AND PROSPECTS

This study reports the detection of a photospheric magnetic field on the FK Com giant HD 199178. The spatial distribution of the field is reconstructed by means of ZDI. The magnetic topology of HD 199178 presents at all observing epochs large regions in which field lines are mostly azimuthally oriented. This observation, together with similar ones reported for other fast rotators (Donati et al. 2003a), suggests that the dynamo processes generating the magnetic activity of HD 199178 may be active very close to the stellar surface.

Local short-term evolution of surface brightness and magnetic structures are observed on time-scales as short as a couple of weeks. A polarity reversal is reported during the summer of 2002 for high-latitude magnetic regions hosting a radial field. A slow increase of the fraction of magnetic energy stored at low-latitude in the large-scale azimuthal component is also observed. Beside these local evolutions, the largest features of the brightness and magnetic topologies remain stable over several years. Although the observed surface changes remain mostly limited to small structures on our 4.5-yr monitoring, future observations may tell us whether the magnetic field of HD 199178 undergoes a cyclical evolution similar to that observed on the Sun.

It is finally suggested that the surface of HD 199178 is sheared by a solar-like differential rotation. The difference in rotation rate between equatorial and polar regions is reported to be about 1.5 times that of the Sun.

The observations reported here are at the limit of the capacity of the MuSiCoS spectropolarimeter, in terms of S/N and spectral resolution. Much more accurate observations are therefore expected

for the same star when the new generation of spectropolarimeters becomes available, with ESPaDOnS at the Canada–France–Hawaii Telescope (Donati 2003) and NARVAL at TBL (Aurière 2003). Better data may in particular allow us to probe more discreet photospheric effects, like possible secular fluctuations in the amount of differential rotation, as already reported for other active stars (Donati et al. 2003b).

ACKNOWLEDGMENTS

PP thanks the Portuguese Fundação para a Ciência e a Tecnologia for grant support # SFRH/BPD/11139/2002. GAW and JDL acknowledge grant support from the Natural Sciences and Engineering Research Council of Canada (NSERC). JMO acknowledges support of the UK Particle Physics and Astronomy Research Council (PPARC). We thank the anonymous referee whose comments helped to improve the manuscript.

REFERENCES

Aurière M., 2003, in Arnaud J., Meunier N., eds, EAS Publ. Ser., 9, 105
Barnes J. R., Collier Cameron A., Unruh Y. C., Donati J. F., Hussain G. A. J., 1998, MNRAS, 299, 904
Baudrand J., Böhm T., 1992, A&A, 259, 711
Bopp B. W., Stencel R. E., 1981, ApJL, 247, L131
Brown S. F., Donati J.-F., Rees D. E., Semel M., 1991, A&A, 250, 463
Cameron A. C., 1992, in Byrne P. B., Mullan D. J. eds, Surface Inhomogeneities on Late-Type Stars. Springer, Berlin, p. 33
Cameron A. C., 2002, Astron. Nachr., 323, 336
Cameron A. C., Unruh Y. C., 1994, MNRAS, 269, 814
Cattaneo F., 1999, ApJ, 515, L39
Corbard T., Thompson M. J., 2002, Sol. Phys., 205, 211
Dikpati M., Gilman P. A., 2001, ApJ, 559, 428
Dikpati M., Corbard T., Thompson M. J., Gilman P. A., 2002, ApJ, 575, L41
Donati J.-F., 1999, MNRAS, 302, 457
Donati J.-F., 2003, in Trujillo-Bueno J., Stenflo J., eds, ASP Conf. Ser, Solar Polarization. Astron. Soc. Pac., San Francisco, in press
Donati J.-F., Brown S. F., 1997, A&A, 326, 1135
Donati J.-F., Cameron A. C., 1997, MNRAS, 291, 1
Donati J.-F., Semel M., Carter B. D., Rees D. E., Cameron A. C., 1997, MNRAS, 291, 658
Donati J.-F., Catala C., Wade G. A., Gallou G., Delaigue G., Rabou P., 1999, A&AS, 134, 149
Donati J.-F., Cameron A. C., Semel M. et al., 2003a, MNRAS, 345, 1145
Donati J.-F., Cameron A. C., Petit P., 2003b, MNRAS, 345, 1187
Hackman T., Jetsu L., Tuominen I., 2001, A&A, 374, 171
Hale G. E., 1908, ApJ, 28, 315
Jetsu L., Pelt J., Tuominen I., Nations H., 1991, in Tuominen I., Moss D., Rudiger G., eds, The Sun and Cool Stars. Activity, Magnetism, Dynamos. Proc. Colloquium No. 130 of the International Astronomical Union. Springer-Verlag, Berlin, p. 381
Kitchatinov L. L., Rüdiger G., 1999, A&A, 344, 911
Korhonen H., Berdyugina S. V., Tuominen I., 2002, A&A, 390, 179
Küker M., Stix M., 2001, A&A, 366, 668
O'Neal D., Neff J. E., Saar S. H., 1998, ApJ, 507, 919
Petit P., Donati J.-F., Cameron A. C., 2002, MNRAS, 334, 374
Petit P. et al., 2004, MNRAS, 348, 1175
Reiners A., Schmitt J. H. M. M., 2002, A&A, 393, L77
Rempel M., Schüssler M., Tóth G., 2000, A&A, 363, 789
Schou J. et al., 1998, ApJ, 505, 390
Semel M., 1989, A&A, 225, 456
Skilling J., Bryan R. K., 1984, MNRAS, 211, 111
Solanki S. K., 2001, ASP Conf. Ser. Vol. 248, Magnetic Fields Across the Hertzsprung–Russell Diagram. Astron. Soc. Pac., San Francisco, p. 45
Strassmeier K. G., Lupinek S., Dempsey R. C., Rice J. B., 1999, A&A, 347, 212
Unruh Y. C., Cameron A. C., 1995, MNRAS, 273, 1
Wade G. A., Donati J.-F., Landstreet J. D., Shorlin S. L. S., 2000, MNRAS, 313, 823

This paper has been typeset from a TEX/LATEX file prepared by the author.